Efficient $\mathcal{O}(N^2)$ method to solve the Bethe-Salpeter equation

W. G. Schmidt,* S. Glutsch, P. H. Hahn, and F. Bechstedt
Institut für Festkörpertheorie und Theoretische Optik, Friedrich-Schiller-Universität Jena, Max-Wien-Platz 1, 07743 Jena, Germany
(Received 3 October 2002; published 6 February 2003)

We present a numerically efficient approach to solve the Bethe-Salpeter equation for the polarization function. Rather than from the usual eigenvalue representation, the macroscopic polarizability is obtained from the solution of an initial-value problem. This reduces the computational effort considerably and allows for calculating excitonic and local-field effects in optical spectra of complex systems consisting of many atoms. As an example we investigate the optical anisotropy of the monohydride Si(001)(2×1) surface. While excitonic effects influence the surface optical properties considerably, the local-field effect induced changes are minimal.

DOI: 10.1103/PhysRevB.67.085307 PACS number(s): 73.20.At, 78.68.+m, 71.15.Qe

I. INTRODUCTION

Recent years have seen impressive methodological progress in the accurate numerical modeling of optical properties from first principles (see, e.g., Ref. 1). It has become possible not only to calculate single-particle electronic excitation energies accurately using the *GW* approximation (GWA), but also to solve the Bethe-Salpeter equation (BSE) for pair excitations in order to account for excitonic and local-field (LF) contributions to the optical response.[2–4] However, the large numerical effort required to solve the BSE has restricted such calculations to the interaction of relatively few electron-hole pairs. Therefore its application has been limited to bulk semiconductors,[2,3,5] strongly localized surface states,[6,7] small clusters,[8] or molecules.[9]

At the same time, methods of optical spectroscopy are rapidly gaining importance for materials characterization. Techniques such as reflectance anisotropy spectroscopy (RAS) have evolved from experimental methods to characterize static surfaces to very powerful *in situ* diagnostic probes which allow for the monitoring and controlling of surface growth in real time and in challenging environments such as in high pressures or under liquids.[10] In order to fully exploit the potential of such methods, however, the accurate theoretical modeling of the optical properties of large and complex systems—such as surfaces—is required. A number of technical improvements such as optimized schemes to calculate the electron-hole interaction in reciprocal space[11] and methodological developments which allow to obtain the polarization function from iterative schemes[12] have been suggested in order to extend the applicability of the BSE to larger and potentially more interesting systems.

In the present work we suggest an alternative approach to solve the BSE. It is characterized by a $\mathcal{O}(N^2)$ scaling of the operation count (with N being the number of electron-hole pair states) and allows for the accurate modeling of excitonic and LF effects in systems consisting of comparatively many atoms. After a brief description of the proposed methodology and its test for bulk Si we demonstrate its applicability to large systems by calculating the optical anisotropy of the monohydride Si(001)(2×1) surface in a wide spectral range.

II. METHODOLOGY

We start from first-principles pseudopotential calculations, using a massively parallel real-space finite-difference implementation of the density-functional theory in local-density approximation (DFT-LDA).[13] A multigrid technique is used for convergence acceleration. In order to include electronic self-energy effects one needs to replace the local exchange and correlation potential $V^{XC}(\mathbf{r})$ in the LDA by the nonlocal and energy-dependent self-energy operator $\Sigma(\mathbf{r},\mathbf{r}';E)$ (see, e.g., Refs. 14 and 15). For the calculation of Σ we use the *GW* approximation,[16,17] where the self-energy operator is expressed as the convolution $\Sigma = iGW$ of the dynamically screened Coulomb potential W and the single-particle propagator G. Since the calculation of surface optical spectra involves a very large number of electronic states, however, we introduce further approximations following the schemes developed by Hybertsen and Louie[18] and Bechstedt *et al.*:[19] the *GW* quasiparticle energies are obtained from the DFT-LDA eigenvalues in a perturbative manner by

$$\varepsilon_n(\mathbf{k})^{QP} = \varepsilon_n(\mathbf{k}) + \frac{1}{1+\beta_{n,\mathbf{k}}}\{\Sigma^{st}_{n,\mathbf{k}} + \Sigma^{dyn}_{n,\mathbf{k}}[\varepsilon_n(\mathbf{k})] - V^{XC}_{n,\mathbf{k}}\}, \tag{1}$$

where the self-energy operator Σ has been divided into static (st) and dynamic (dyn) contributions. Indices at Σ and V^{XC} indicate diagonal matrix elements with the respective wave functions. $\beta_{n,\mathbf{k}}$ is the linear coefficient in the expansion of Σ^{dyn} around the DFT-LDA eigenvalue $\varepsilon_n(\mathbf{k})$. The static part can be further divided into two parts,

$$\Sigma^{st}(\mathbf{r},\mathbf{r}') = \frac{1}{2}\sum_{n,\mathbf{k}} \psi_{n,\mathbf{k}}(\mathbf{r})\psi^*_{n,\mathbf{k}}(\mathbf{r}')[W(\mathbf{r},\mathbf{r}';0) - v(\mathbf{r}-\mathbf{r}')] - \sum_{v,\mathbf{k}} \psi_{v,\mathbf{k}}(\mathbf{r})\psi^*_{v,\mathbf{k}}(\mathbf{r}')W(\mathbf{r},\mathbf{r}';0), \tag{2}$$

representing the Coulomb hole Σ^{COH} and the screened exchange Σ^{SEX}. The $\psi_{n,\mathbf{k}}$ are the DFT-LDA wave functions. Σ^{SEX} contains a sum over the occupied valence states v only. The major bottleneck in the *GW* calculation is the computation of the screened interaction W. An extreme acceleration can be achieved by using a model dielectric function, for which several functional forms have been suggested. We use the version suggested by Bechstedt *et al.*[19]

$$\epsilon(\mathbf{q},\rho)=1+\left\{(\epsilon_\infty-1)^{-1}+\left[\frac{q}{q_{TF}(\rho)}\right]^2+\frac{3q^4}{4k_F^2(\rho)q_{TF}^2(\rho)}\right\}^{-1}, \tag{3}$$

where k_F and q_{TF} represent the Fermi and Thomas-Fermi wave vectors, respectively, which depend on the electron density ρ. This expression interpolates between the correct behaviors at high and low $\mathbf{q}$ vectors and, by construction, correctly obtains the static dielectric constant for $\mathbf{q}=0$. This rather simple and intuitive model reproduces very well the random-phase approximation results for semiconductors.[20] Together with the LDA-like ansatz of Hybertsen and Louie[18] for approximating the spatial dependence of the screening of the inhomogeneous system

$$W(\mathbf{r},\mathbf{r}';0)=\frac{1}{2}\{W^h[\mathbf{r}-\mathbf{r}',\rho(\mathbf{r})]+W^h[\mathbf{r}-\mathbf{r}',\rho(\mathbf{r}')]\} \tag{4}$$

by that of a homogeneous electron gas W^h, Eq. (3) allows for an analytic solution for Σ_{COH}. The static Coulomb hole contribution to the self-energy takes the form of a local potential,

$$\Sigma^{COH}(\mathbf{r})=-\frac{q_{TF}(\mathbf{r})}{2}\sqrt{1-\frac{1}{\epsilon_\infty}}\left[1+\frac{q_{TF}(\mathbf{r})}{k_F(\mathbf{r})}\sqrt{\frac{3\epsilon_\infty}{\epsilon_\infty-1}}\right]^{-1/2}, \tag{5}$$

where k_F and q_{TF} are computed at the local density $\rho(\mathbf{r})$.

The matrix elements $\Sigma^{SEX}_{n,\mathbf{k}}$ are calculated in Fourier space. In order to accelerate the calculations, only the diagonal elements in the Fourier transform of W are retained. The effect of local fields on the screening are approximated by using state-averaged electron densities,

$$\rho_{n,\mathbf{k}}=\int d\mathbf{r}^3\rho(\mathbf{r})|\psi_{n,\mathbf{k}}(\mathbf{r})|^2, \tag{6}$$

in the calculation of k_F and q_{TF}.[19] Tests made for Si indicate that rather small deviations, of the order of 0.05 eV, are induced by this approximation, at least for bulk crystals with moderate electron-density fluctuations. Finally, the dynamic terms $\beta_{n,\mathbf{k}}$ and Σ^{dyn} in Eq. (1) are approximated by simple integrals of the dielectric function.[19] For the actual calculations we use Eq. (3) together with a single-plasmon-pole approximation to describe the frequency dependence. Local-field effects are again included using the mean-density approximation (6). The integrals are numerically evaluated for a dense sampling of ρ and the results for $\beta_{n,\mathbf{k}}(\rho)$ and $\Sigma^{dyn}(\rho)$ are fitted to polynomials. These are then used for a fast computation of the dynamic contributions to the self-energy during the actual GW calculations. For several III-V compounds and their surfaces this approximate treatment of self-energy corrections has been shown to result in excitation energies which are within about 0.1 eV of the experimental values.[21–23]

Excitation energies obtained within the quasiparticle formalism describe one-particle excitations, such as those involved in direct or inverse photoemission experiments. For the description of the optical absorption, however, one needs to go beyond this single-quasiparticle level. The polarization function P including electron-hole attraction and local-field effects (or electron-hole exchange) can be obtained from the solution of the Bethe-Salpeter equation (for details see, e.g., Refs. 24–27),

$$P=P_0+P_0(\bar{v}-W)P, \tag{7}$$

where $\bar{v}$ is the bare Coulomb potential without its long-range part and P_0 represents the polarization function in a random-phase, or, more precisely, independent-quasiparticle approximation. The macroscopic polarizability is obtained from the Fourier transform of the diagonal part of P.

A convenient and natural basis for solving Eq. (7) is given by the orthonormal and complete set of Bloch functions defined by the Kohn-Sham problem. If P_0 is explicitly expressed in terms of Bloch functions and quasiparticle energies and transformed into Bloch space, the solution of the BSE (7) can be written in resolvent representation as

$$P_{(n_1,n_2)(n_3,n_4)}=[\hat{H}-\omega]^{-1}_{(n_1,n_2)(n_3,n_4)}(f_{n_4}-f_{n_3}), \tag{8}$$

where the two-particle Hamiltonian

$$\begin{aligned}\hat{H}_{(n_1,n_2)(n_3,n_4)}&\equiv(\varepsilon^{QP}_{n_1}-\varepsilon^{QP}_{n_2})\delta_{(n_1,n_3)}\delta_{(n_2,n_4)}+(f_{n_2}-f_{n_1})\\&\times\int d\mathbf{r}_1d\mathbf{r}_2d\mathbf{r}_3d\mathbf{r}_4\psi_{n_1}(\mathbf{r}_1)\psi^*_{n_2}(\mathbf{r}_2)\psi^*_{n_3}(\mathbf{r}_3)\psi_{n_4}(\mathbf{r}_4)\\&\times[\delta(\mathbf{r}_1-\mathbf{r}_2)\delta(\mathbf{r}_3-\mathbf{r}_4)\bar{v}(\mathbf{r}_1-\mathbf{r}_3)\\&-\delta(\mathbf{r}_1-\mathbf{r}_3)\delta(\mathbf{r}_2-\mathbf{r}_4)W(\mathbf{r}_1,\mathbf{r}_2)]\end{aligned} \tag{9}$$

has been introduced. $f_n=0,1$ is the occupation number of the state n, denoting both band index and wave vector. By performing a matrix inversion for a given frequency ω, the corresponding polarization is given by Eq. (8). However, for any practical calculation this would be computationally far too expensive, due to the non-Hermiticity and large dimension of $\hat{H}$. The dimension can be reduced by a factor of 2, however, if one observes that due to the factors $(f_{n_4}-f_{n_3})$ in Eq. (8) and $(f_{n_2}-f_{n_1})$ in Eq. (9), only pairs containing one filled and one empty Bloch state contribute to the macroscopic polarization. A further reduction of the dimension by a factor of 2 can be achieved when the off-diagonal blocks, which couple the Hermitian resonant part of $\hat{H}$,

$$\begin{aligned}\hat{H}^{res}_{vc\mathbf{k},v'c'\mathbf{k}'}&=(\varepsilon^{QP}_{c\mathbf{k}}-\varepsilon^{QP}_{v\mathbf{k}})\delta_{vv'}\delta_{cc'}\delta_{\mathbf{k},\mathbf{k}'}\\&+2\int d\mathbf{r}_1d\mathbf{r}_2\psi^*_{c\mathbf{k}}(\mathbf{r}_1)\psi_{v\mathbf{k}}(\mathbf{r}_1)\bar{v}(\mathbf{r}_1-\mathbf{r}_2)\\&\times\psi_{c'\mathbf{k}'}(\mathbf{r}_2)\psi^*_{v'\mathbf{k}'}(\mathbf{r}_2)\\&-\int d\mathbf{r}_1d\mathbf{r}_2\psi^*_{c\mathbf{k}}(\mathbf{r}_1)\psi_{c'\mathbf{k}'}(\mathbf{r}_1)W(\mathbf{r}_1,\mathbf{r}_2)\\&\times\psi_{v\mathbf{k}}(\mathbf{r}_2)\psi^*_{v'\mathbf{k}'}(\mathbf{r}_2),\end{aligned} \tag{10}$$

and the antiresonant part, $-[\hat{H}^{res}]^*$, are neglected. The coupling blocks with contributions only from the interaction

terms involving W and $\bar{v}$ are small compared to the (anti-) resonant diagonal blocks containing in addition the quasiparticle transition energies. Apart from special cases, e.g., the calculation of plasmon resonances where the mixing of interband transitions of both positive and negative frequencies must be included in the calculations,[28] the coupling can be neglected in the calculation of optical properties.[2,29] Further approximations in Eq. (10) are the restriction to spin singlets, static screening and direct transitions, i.e., the neglect of momentum transfer by photons. Furthermore if umklapp processes are neglected, the exciton Hamiltonian can be calculated in reciprocal space according to

$$\begin{aligned}\hat{H}^{res}_{vc\mathbf{k},v'c'\mathbf{k}'} &= (\varepsilon^{QP}_{c\mathbf{k}} - \varepsilon^{QP}_{v\mathbf{k}})\delta_{vv'}\delta_{cc'}\delta_{\mathbf{kk}'} \\ &+ \frac{4\pi}{\Omega}\sum_{\mathbf{G},\mathbf{G}'}\left\{ 2\frac{\delta_{\mathbf{GG}'}(1-\delta_{\mathbf{G}0})}{|\mathbf{G}|^2} B^{\mathbf{kk}}_{cv}(\mathbf{G}) B^{\mathbf{k}'\mathbf{k}'}_{c'v'}{}^{*}(\mathbf{G}) \right. \\ &- \frac{\epsilon^{-1}(\mathbf{k}-\mathbf{k}'+\mathbf{G},\mathbf{k}-\mathbf{k}'+\mathbf{G}',0)}{|\mathbf{k}-\mathbf{k}'+\mathbf{G}|^2} \\ &\left. \times B^{\mathbf{kk}'}_{cc'}(\mathbf{G}) B^{\mathbf{kk}'}_{vv'}{}^{*}(\mathbf{G}') \right\}, \end{aligned} \tag{11}$$

where the Bloch integral

$$B^{\mathbf{kk}'}_{nn'}(\mathbf{G}) = \frac{1}{\Omega}\int d\mathbf{r} u^{*}_{n\mathbf{k}}(\mathbf{r}) e^{i\mathbf{G}\mathbf{r}} u_{n'\mathbf{k}'}(\mathbf{r}) \tag{12}$$

over the periodic parts u of the Bloch wave functions has been introduced and Ω denotes the volume of the unit cell.

The calculation of the Hamiltonian according to Eq. (11) is computationally very demanding even for bulk systems, due to the rank N of the Hamiltonian itself, as well as due to the double sum over $\mathbf{G}$ and $\mathbf{G}'$, which needs to be performed for each single matrix element. The number of pair states is proportional to the number of valence bands N_v, conduction bands N_c, and the number $N_{\mathbf{k}}$ of mesh points in $\mathbf{k}$ space, $N = N_v \cdot N_c \cdot N_{\mathbf{k}}$. In order to speed up the calculations, we therefore replace the inverse dielectric matrix by the same diagonal model dielectric function of Bechstedt (3), which has been used in the calculation of the self-energy operator. The influence of the off-diagonal elements is again approximated by using state-dependent electron densities in Eq. (3), which were calculated using the mean-density approximation (6).

After the Hamiltonian has been calculated, one needs to determine the frequency-dependent polarizability. The rank of $\hat{H}$ depends on the spectral region that is studied. It is typically of the order of 10^4 even for small bulk unit cells. The large number of pair states excludes the straightforward evaluation of Eq. (8). The usual approach therefore consists of transforming the calculation of the resolvent into an effective eigenvalue problem, which is then solved by diagonalization.[2,8] In detail, using the spectral representation

$$[\hat{H}-\omega]^{-1} = \sum_{\lambda,\lambda'} \frac{|A^{\lambda}\rangle S^{-1}_{\lambda,\lambda'}\langle A^{\lambda'}|}{E_{\lambda}-w}, \tag{13}$$

where $|A^{\lambda}\rangle$ and E_{λ} are the eigenvectors and eigenvalues of the exciton Hamiltonians

$$\hat{H}|A^{\lambda}\rangle = E_{\lambda}|A^{\lambda}\rangle, \quad S_{\lambda,\lambda'} = \langle A^{\lambda'}|A^{\lambda}\rangle, \tag{14}$$

the diagonal components of the macroscopic polarizability are given by

$$\begin{aligned}\alpha^{M}_{jj}(\omega) = \frac{4e^2\hbar^2}{\Omega}\sum_{\lambda}\left|\sum_{\mathbf{k}}\sum_{c,v}\frac{\langle c\mathbf{k}|v_j|v\mathbf{k}\rangle}{\varepsilon_c(\mathbf{k})-\varepsilon_v(\mathbf{k})}A^{\lambda}_{vc\mathbf{k}}\right|^2 \\ \times\left\{\frac{1}{E_{\lambda}-\hbar(\omega+i\gamma)}+\frac{1}{E_{\lambda}+\hbar(\omega+i\gamma)}\right\}, \end{aligned} \tag{15}$$

where v_j is the corresponding Cartesian component of the single-particle velocity operator and γ the damping constant. Here, the contributions of the antiresonant part of the exciton Hamiltonian have been formally included, while the coupling parts are neglected.

The calculation of the polarizability using Eq. (15) is straightforward, but requires the solution of the eigenvalue problem (14). For small bulk unit cells the diagonalization of $\hat{H}$ can typically be performed within a couple of CPU time hours. However, our work aims at determining of optical properties for large and complex systems. The minimum slab thickness for the calculation of surface optical properties, for example, is about 12 layers. Typically more than 100 $\mathbf{k}$ points are needed to sample the surface Brillouin zone. About two valence and conduction bands per atom need to be taken into account in order to cover a spectral region of several eV. The dimension of the exciton Hamiltonian $N = N_v \cdot N_c \cdot N_{\mathbf{k}}$ is therefore about $10^5 \ldots 10^6$, already for the relatively small unit cell of an unreconstructed surface. Even with today's powerful supercomputers, the diagonalization of matrices of this size, which scales as $\mathcal{O}(N^3)$, is prohibitively slow.

Therefore, we formulate the calculation of the ω-dependent polarizability as an initial-value problem. If a vector $|\mu^j\rangle$ of dipole moments with elements

$$\mu^{j}_{vc\mathbf{k}} = \frac{\langle c\mathbf{k}|v_j|v\mathbf{k}\rangle}{\varepsilon_c(\mathbf{k})-\varepsilon_v(\mathbf{k})} \tag{16}$$

is introduced, Eq. (15) takes the form

$$\begin{aligned}\alpha^{M}_{jj}(\omega) = \frac{4e^2\hbar^2}{\Omega}\sum_{\lambda}|\langle\mu^j|A^{\lambda}\rangle|^2\left\{\frac{1}{E_{\lambda}-\hbar(\omega+i\gamma)}\right. \\ \left.+\frac{1}{E_{\lambda}+\hbar(\omega+i\gamma)}\right\}. \end{aligned} \tag{17}$$

This is equivalent to the Fourier representation

$$\alpha^{M}_{jj}(\omega) = \frac{4e^2\hbar^2}{\Omega} i\int_0^{\infty} dt e^{i(\omega+i\gamma)t}\{\langle\mu^j|\xi^j(t)\rangle - \langle\mu^j|\xi^j(t)\rangle^{*}\}, \tag{18}$$

where the time evolution of the vector $|\xi^j(t)\rangle$ is driven by the pair Hamiltonian

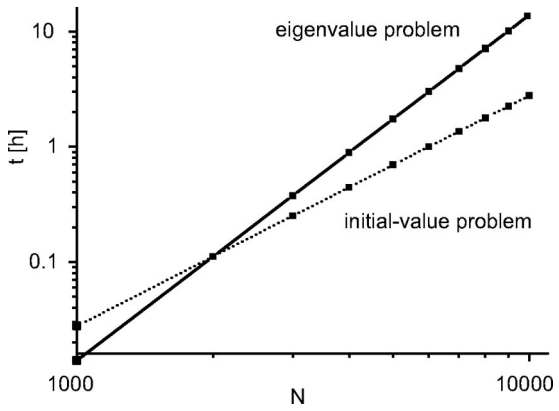

FIG. 1. CPU time needed to solve the BSE for bulk Si as an eigenvalue and as an initial-value problem on a single-processor Pentium PC dependent on the dimension $N=N_v\cdot N_c\cdot N_{\mathbf{k}}$ of the exciton Hamiltonian.

$$i\hbar\frac{d}{dt}|\xi^j(t)\rangle=\hat{H}|\xi^j(t)\rangle \tag{19}$$

and the initial vector elements are given by

$$|\xi^j(0)\rangle=|\mu^j\rangle. \tag{20}$$

The equivalence (see also Ref. 30) can be shown by integrating $|\xi(t)\rangle=e^{\hat{H}t/i\hbar}|\mu\rangle$ and exploiting the spectral representation as in Eq. (13). We have also verified numerically that Eqs. (17) and (18) lead to exactly the same spectrum.[31] The latter formula, however, requires much less computational resources. We solve the initial-value problem defined by Eqs. (19) and (20) using the central-difference method (see, e.g., Ref. 32) which obtains $|\xi(t_{i+2})\rangle$ from $|\xi(t_i)\rangle$ and $|\xi(t_{i+1})\rangle$ by an explicit scheme,

$$\hat{H}|\xi(t_{i+1})\rangle=i\hbar\frac{|\xi(t_{i+2})\rangle-|\xi(t_i)\rangle}{2\Delta t}. \tag{21}$$

This procedure only requires one matrix-vector multiplication per time step. The stability of the difference scheme (21) requires that $\Delta t<\hbar/||\hat{H}||$. The upper limit of the Fourier integral (18) can be truncated, due to the exponential $e^{-\gamma t}$. Therefore, the number of time steps, i.e., matrix-vector multiplications, is nearly independent of the dimension of the system and governed by γ. The order of 10^3 time steps are typically required using a broadening parameter $\gamma=0.1$ eV. The operation count for this method scales thus as $\mathcal{O}(N^2)$, compared to $\mathcal{O}(N^3)$ for the matrix diagonalization. The crossover point for CPU time usage of both methods in our implementation is reached for a number of electron-hole pair states as low as about 2000 for a single processor (see Fig. 1). Moreover, the matrix-vector multiplications can be easily distributed on several processors of a parallel computer, whereas the parallelization of matrix diagonalization is less effective, due to the large amount of data transfer across processors.

As an example, the time-dependent polarizability calculated for bulk Si is plotted in Fig. 2. It is reminiscent of the interference of two oscillators with different resonance frequencies. The imaginary part of the corresponding frequency-dependent dielectric function is shown in Fig. 3. Here the influence of electronic self-energy effects calculated in the GWA and of excitonic and local-field effects obtained from the solution of the BSE are shown separately. Compared to the DFT-LDA spectrum (i.e., the spectrum in the approximation of independent Kohn-Sham particles), the self-energy corrections lead to a blueshift of the characteristic peaks corresponding to the E_1 and E_2 critical point energies. The line shape is only slightly affected. However, similar to previous works,[2,5] a strong redistribution of oscillator strength from the E_2 peak and partially from the high-energy peak at about 5.5 eV to the E_1 energy accompanied by a slight redshift is observed upon solving the BSE. However, the calculated peak positions still occur at energies that are about 0.2 eV too high. Our calculations were performed at the theoretical equilibrium lattice constant of 5.378 Å. That leads to an increase of the energy splitting between occupied and empty states by about 0.1 eV compared to calculations at the experimental lattice constant. In addition, temperature effects in the measured spectrum[33] result in a redshift by about 0.05 eV.[34] This shift is not included in the zero-temperature calculations, which use, however, a broadening parameter $\gamma=0.15$ eV in order to account for the finite number of $\mathbf{k}$ points. Thus, despite the numerous simplifications used in the present approach, the solution of the BSE for

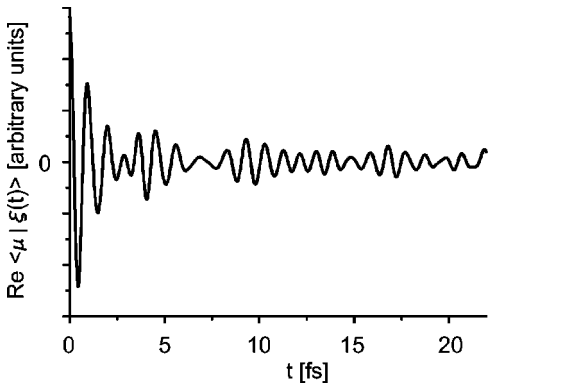

FIG. 2. Time evolution of the polarizability $\Re\langle\mu|\xi(t)\rangle$ calculated for bulk Si according to Eqs. (19) and (20).

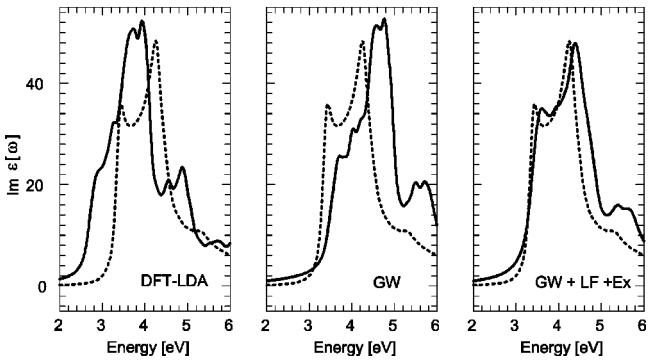

FIG. 3. Dielectric function (imaginary part) of bulk Si calculated within the DFT-LDA, in GW approximation, and from the BSE (GW+LF and excitonic effects) in comparison with the experimental data from Ref. 33 (dotted line).

bulk Si yields an optical spectrum in nearly perfect agreement with experiment. The experimental results are seemingly even better reproduced than in previous calculations,[2] where the screening has been fully included. That is simply related to the fact that the approximations made here allow for a better convergence of the technical parameters. The discrepancies between experiment and theory discussed in Refs. 2 and 35, for example, are related to the insufficient **k**-point sampling.[36] The optical spectra shown in Fig. 3 were calculated using a mesh of 4000 **k** points uniformly distributed in the whole bulk Brillouin zone.

III. APPLICATION TO THE MONOHYDRIDE Si(001)(2×1) SURFACE

Surfaces are complex systems and usually need to be described by slabs containing several dozen atoms. In some special cases, e.g., for Si(111)(2×1) or Ge(111)(2×1) surfaces,[6,7] certain surface optical features are solely determined by a few surface bands within the region of the fundamental gap. More often, however, and in particular if a wide spectral range is considered, surface-modified bulk states also contribute to the surface optical response. This is the case for the hydrogenated Si(001) surface, where the dimer-related surface states have been removed from the fundamental gap region and the characteristic spectral features appear at the energies of the bulk critical points. Consequently, a large number of electron-hole pairs need to be included in the calculation. Therefore, this surface is a suitable test case for our method.

The nominal (2×1) reconstructed Si(001) surface typically has both (2×1) and (1×2) reconstructed domains, the optical anisotropy of which cancels. In order to obtain a single-domain surface, and in order to minimize at the same time optical anisotropies due to surface steps,[37] Shioda and van der Weide used electromigration to prepare an atomically flat, single-domain monohydride-terminated Si(001)(2×1) surface.[38] Its measured normal-incidence surface optical anisotropy

$$\frac{\Delta r}{r}(\omega)=2\Re\left\{\frac{r_{[\bar{1}10]}-r_{[110]}}{r_{[\bar{1}10]}-r_{[110]}}\right\} \tag{22}$$

is shown in Fig. 4. Here $r_{[\bar{1}10]}(\omega)$ and $r_{[110]}(\omega)$ denote the complex reflectivities for light polarized parallel and perpendicular, respectively, to the dimer row of the majority domain. The measured signal is characterized by positive and negative peaks around 3.4 (A′) and 4.3 (B′) eV. At these energies, the critical points of the bulk electronic responses, the E_1 and E_2 structures occur.[33] Therefore, the optical anisotropy of the hydrogen-terminated Si(001) surface is explained as modulation of the bulk dielectric function. The peak around 3.4 eV has also been observed in an earlier study by Müller *et al.*,[39] who used a wet process to prepare the surface.

Computationally, the monohydride Si(001) surface is modeled in our study by a slab containing 12 atomic Si(001) layers. Both sides of the slab are hydrogen terminated. A vacuum region equivalent to 12 atomic layers in thickness

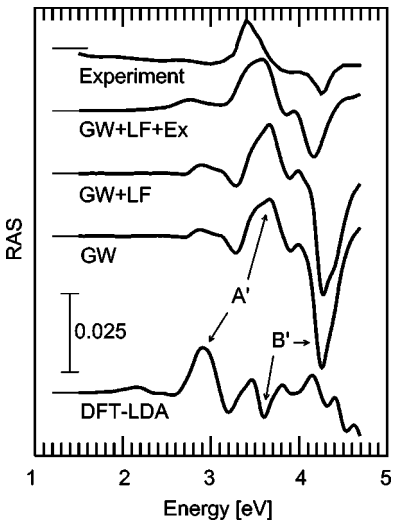

FIG. 4. RAS spectra calculated (within the DFT-LDA, in the *GW* approximation, in the GWA with the effects of local fields included, and in GWA with the effects of local fields and the electron-hole attraction included) for the monohydride Si(001)(2×1) surface are compared with the measured data from Ref. 38.

separates the material slabs in the [001] direction. Apart from the atoms of the innermost two layers, which were kept in their ideal bulk positions, all atomic coordinates are fully relaxed. Four **k** points in the irreducible part of the surface Brillouin zone are used for the self-consistent calculation of the ground-state charge density. For the calculation of the surface optical properties we use 200 uniformly distributed **k** points. Further numerical details of the DFT-LDA calculations are like those in our previous works on the optical response of Si(111):H and Si(001) surfaces.[37,40] The reflectance anisotropy for normally incident light polarized parallel to the $[\bar{1}10]$ and [110] directions is given by[41,42]

$$\frac{\Delta r}{r}(\omega)=\frac{8\pi\omega}{c}\Im\left\{\frac{\alpha^{hs}_{[\bar{1}10]}(\omega)-\alpha^{hs}_{[110]}(\omega)}{\epsilon_b(\omega)-1}\right\}. \tag{23}$$

Here $\alpha^{hs}_j(\omega)$ with $j=[\bar{1}10],[110]$ is the diagonal tensor component of the averaged half-slab polarizability and $\epsilon_b(\omega)$ is the bulk dielectric function. The spectra resulting from the evaluation of Eq. (23) using the half-slab polarizabilities and bulk dielectric functions obtained within the independent-particle approximation, i.e., the DFT-LDA; the independent-quasiparticle approximation, i.e., including self-energy effects in the *GW* approximation; and the BSE, i.e., including local-field and excitonic effects are compared with the measured data in Fig. 4.

The DFT-LDA spectrum in Fig. 4 shows, in principle, the features observed experimentally. However, the calculated A′ and B′ peaks are redshifted in comparison with the experiment by 0.5 and 0.8 eV, respectively. In addition, the B′ optical anisotropy is much smaller than measured. Self-energy corrections calculated in the *GW* approximation shift the excitation energies to larger values. Now the calculated A′ and B′ peaks occur at 3.65 and 4.25 eV, respectively. Furthermore, the B′ optical anisotropy is much increased.

This is not only related to the nonuniform self-energy corrections of the DFT-LDA eigenvalues, but is also a consequence of the ω scaling of the optical anisotropy in Eq. (23).

In order to determine the influence of excitonic and LF effects on the RAS we calculate the exciton Hamiltonian for the surface according to Eq. (11). In the slab calculation 50 valence and 50 conduction bands at 200 **k** points are taken into account. This would give rise to a rank $N=N_v \cdot N_c \cdot N_{\mathbf{k}} = 500\,000$ of the electron-hole pair Hamiltonian (10). Fortunately, however, it turns out that not all matrix elements are needed to calculate a numerically converged optical spectrum for the photon energies considered here. Using an energy cutoff we could reduce the rank of the Hamiltonian to 100 000. Still, the calculation of the matrix elements requires an appreciable amount of computer time, about 20 000 node hours. The task was solved by parallelizing the calculation, using 128 Cray T3E processors. The calculation of the polarization itself, using the central-difference method (21), is highly efficient. It requires only about 2000 node hours. This shows that now the bottleneck of the calculation is the computation of the Hamiltonian matrix rather than the solution of the BSE. Benedict and Shirley[12] avoid the calculation of the exciton Hamiltonian by using an iterative scheme that only requires computing the Hamiltonian acting on a vector.

It has been discussed for a long time that LF effects contribute substantially to the surface optical anisotropy (see, e.g. Refs. 43 and 44). Surface LF effects can be expected from both the microscopic fluctuations of the electric field within the bulk, and from the truncation of the bulk itself. The numerical calculation for the hydrogenated Si(001) surface, however, shows that LF effects lead to surprisingly small changes of the spectrum, at least in the particular case studied here. A reduction of the calculated slab polarizabilities upon inclusion of LF effects is observed, which is comparable to the one calculated for bulk Si. However, the reduction acts on both the $\alpha_{[\bar{1}10]}$ and the $\alpha_{[110]}$ tensor components. It is therefore largely canceled in the optical anisotropy. Similar findings were recently obtained for the Si(110):H surface.[45]

A distinct change of the RAS spectrum, however, results from the inclusion of the attractive electron-hole interaction. We observe a strong reduction of the B′ optical anisotropy and an increase of the integrated A′ peak area. At the same time, the A′ and B′ optical anisotropies are shifted to lower energies by about 0.2 eV.

The stepwise inclusion of many-particle effects in the calculation leads to a considerable and systematic improvement of the agreement with the experiment. The trends regarding peak positions and oscillator strengths are in accord with the results obtained for Si bulk (cf. Fig. 3). However, the uppermost calculated curve in Fig. 4 still deviates from the measured data. On the one hand, this concerns the line shape. The calculated A′ optical anisotropy is too broad and there are pronounced features in the calculated spectrum at 2.7 and 3.9 eV, where experiment shows only weak shoulders. On the other hand, the calculated peak positions do not agree exactly with experiment. This is to some extent related to the approximations used in the present approach. In particular the approximations used for the off-diagonal elements in the calculation of the screened Coulomb potential W can be expected to lead to a somewhat inaccurate modeling of the highly inhomogeneous screening at the semiconductor surface. Probably more important, however, are the numerical limitations of our study. Well-converged calculations of surface optical properties require thicker slabs and in particular larger **k**-point sets than what could be used in the present study. At least 1024 **k** points in the full (1×1) surface Brillouin zone are needed, for example, to obtain numerically converged optical spectra for Si(001) surfaces (see Fig. 1 in Ref. 37). Despite the efficiency of the present approach for solving the BSE, such a **k**-point density is still out of reach, due to computer memory limitations. Temperature effects in the measured spectrum, which are neglected in our calculations, as well as surface defects, will also result in deviations between experiment and theory.

IV. SUMMARY

We presented an approach for solving the Bethe-Salpeter equation, which is based on a time-evolution technique. It allows for including local-field and electron-hole attraction effects in the calculation of optical properties for complex systems consisting of many atoms. The application to bulk silicon results in nearly perfect agreement with the measured dielectric function. The applicability to large systems has been demonstrated by calculating the optical anisotropy of the monohydride Si(001)(2×1) surface. It is shown that many-body effects, in particular the electronic self-energy and the electron-hole attraction, lead to strong modifications of the surface optical response. In contrast, the spectral modifications due to local-field effects are negligible.

ACKNOWLEDGMENTS

Helpful discussions with V. Olevano and L. Reining are gratefully acknowledged. We thank R. Venus from the Universitätsrechenzentrum Jena for his help with the parallelization of our code. Generous grants of computer time from the Leibniz-Rechenzentrum München, the Höchstleistungsrechenzentrum Stuttgart, and the John von Neumann-Institut Jülich made the numerical calculations possible. The work was supported by the EU Research Training Network NANOPHASE (Grant No. HPRN-CT-2000-00167).

*Electronic address: wgs@ifto.physik.uni-jena.de

[1] G. Onida, L. Reining, and A. Rubio, Rev. Mod. Phys. **74**, 601 (2002).
[2] S. Albrecht, L. Reining, R. Del Sole, and G. Onida, Phys. Rev. Lett. **80**, 4510 (1998).
[3] L. X. Benedict, E. L. Shirley, and R. B. Bohn, Phys. Rev. Lett. **80**, 4514 (1998).
[4] M. Rohlfing and S. G. Louie, Phys. Rev. Lett. **81**, 2312 (1998).
[5] L. X. Benedict, E. L. Shirley, and R. B. Bohn, Phys. Rev. B **57**, R9385 (1998).
[6] M. Rohlfing and S. G. Louie, Phys. Rev. Lett. **83**, 856 (1999).
[7] M. Rohlfing, M. Palummo, G. Onida, and R. Del Sole, Phys. Rev.

Lett. **85**, 5440 (2000).
[8] M. Rohlfing and S. G. Louie, Phys. Rev. Lett. **80**, 3320 (1998).
[9] J. C. Grossman, M. Rohlfing, L. Mitas, S. G. Louie, and M. L. Cohen, Phys. Rev. Lett. **86**, 472 (2001).
[10] D. E. Aspnes, Solid State Commun. **101**, 85 (1997).
[11] M. Rohlfing and S. G. Louie, Phys. Rev. B **62**, 4927 (2000).
[12] L. X. Benedict and E. L. Shirley, Phys. Rev. B **59**, 5441 (1999).
[13] J. Bernholc, E. L. Briggs, C. Bungaro, M. B. Nardelli, J. L. Fattebert, K. Rapcewicz, C. Roland, W. G. Schmidt, and Q. Zhao, Phys. Status Solidi B **217**, 685 (2000).
[14] F. Bechstedt, *Festköperprobleme/Advances in Solid State Physics* (Vieweg, Braunschweig, 1992), Vol. 32, p. 161.
[15] F. Aryasetiawan and O. Gunnarsson, Rep. Prog. Phys. **61**, 237 (1998).
[16] L. Hedin, Phys. Rev. **139**, A769 (1965).
[17] L. Hedin and S. Lundqvist, *Solid State Physics* (Academic, New York, 1969), Vol. 23, p. 1.
[18] M. S. Hybertsen and S. G. Louie, Phys. Rev. B **37**, 2733 (1988).
[19] F. Bechstedt, R. Del Sole, G. Cappellini, and L. Reining, Solid State Commun. **84**, 765 (1992).
[20] G. Cappellini, R. Del Sole, L. Reining, and F. Bechstedt, Phys. Rev. B **47**, 9892 (1993).
[21] W. G. Schmidt, J. L. Fattebert, J. Bernholc, and F. Bechstedt, Surf. Rev. Lett. **6**, 1159 (1999).
[22] W. G. Schmidt, N. Esser, A.M. Frisch, P. Vogt, J. Bernholc, F. Bechstedt, M. Zorn, T. Hannappel, S. Visbeck, F. Willig, and W. Richter, Phys. Rev. B **61**, R16 335 (2000).
[23] W. G. Schmidt, F. Bechstedt, K. Fleischer, C. Cobet, N. Esser, W. Richter, J. Bernholc, and G. Onida, Phys. Status Solidi A **188**, 1401 (2001).
[24] L. J. Sham and T. M. Rice, Phys. Rev. **144**, 708 (1966).
[25] W. Hanke and L. J. Sham, Phys. Rev. B **21**, 4656 (1980).
[26] G. Strinati, Riv. Nuovo Cimento **11**, 1 (1988).
[27] H. Stolz, *Einführung in die Vielelektronentheorie der Kristalle* (Akademie-Verlag, Berlin, 1974).
[28] V. Olevano and L. Reining, Phys. Rev. Lett. **86**, 5962 (2001).
[29] S. Albrecht, Ph.D. thesis, Ecole Polytechnique, 1999.
[30] D. Weaire, D. Hobbs, G.J. Morgan, J.M. Holender, and F. Wooten, J. Non-Cryst. Solids **166**, 877 (1993); S. Glutsch, D. S. Chemla, and F. Bechstedt, Phys. Rev. B **54**, 11 592 (1996).
[31] P. H. Hahn, Diplomarbeit, Friedrich-Schiller-Universität Jena, 2001.
[32] R. Kosloff, J. Chem. Phys. **92**, 2087 (1988).
[33] D. E. Aspnes and A. A. Studna, Phys. Rev. B **27**, 985 (1983).
[34] P. Lautenschlager, M. Garriga, L. Viña, and M. Cardona, Phys. Rev. B **36**, 4821 (1987).
[35] M. Cardona, L. F. Lastras-Martinez, and D. E. Aspnes, Phys. Rev. Lett. **83**, 3970 (1999).
[36] S. Albrecht, L. Reining, G. Onida, V. Olevano, and R. Del Sole, Phys. Rev. Lett. **83**, 3971 (1999).
[37] W. G. Schmidt, F. Bechstedt, and J. Bernholc, Phys. Rev. B **63**, 045322 (2001).
[38] R. Shioda and J. van der Weide, Appl. Surf. Sci. **130-132**, 266 (1998).
[39] A. B. Müller, F. Reinhard, U. Resch, W. Richter, K. C. Rose, and U. Rossow, Thin Solid Films **233**, 19 (1993).
[40] W. G. Schmidt and J. Bernholc, Phys. Rev. B **61**, 7604 (2000).
[41] R. Del Sole, Solid State Commun. **37**, 537 (1981).
[42] F. Manghi, R. Del Sole, A. Selloni, and E. Molinari, Phys. Rev. B **41**, 9935 (1990).
[43] W. L. Mochán and R. G. Barrera, Phys. Rev. Lett. **55**, 1192 (1985).
[44] B. S. Mendoza, R. Del Sole, and A. I. Shkrebtii, Phys. Rev. B **57**, R12 709 (1998).
[45] P. H. Hahn, W. G. Schmidt, and F. Bechstedt, Phys. Rev. Lett. **88**, 016402 (2002).